

# An Automatic Unsupervised Classification of MR Images in Alzheimer’s Disease

Xiaojing Long  
Virginia Tech  
Blacksburg, VA 24061  
longxj@vt.edu

Chris Wyatt  
Virginia Tech  
Blacksburg, VA 24061  
clwyatt@vt.edu

## Abstract

*Image-analysis methods play an important role in helping detect brain changes in and diagnosis of Alzheimer’s Disease (AD). In this paper, we propose an automatic unsupervised classification approach to distinguish brain magnetic resonance (MR) images of AD patients from those of elderly normal controls. The symmetric log-domain diffeomorphic demons algorithm, with the properties of symmetry and invertibility, is used to compute the pair-wise registration, whose deformation field is then used to calculate the Riemannian distance between them. The spectral embedding algorithm is performed based on the Riemannian distance matrix to project images onto a low-dimensional space where each image is represented as a point and its neighboring points correspond to images of high anatomical similarity. Finally, the quick shift clustering method is employed in the embedded space to partition the dataset into subgroups. The experiments using the proposed method show very good performance for clustering images into AD and normal aging, using the Clinical Dementia Rating (CDR) scale as a comparison.*

**Abbreviations:** AD, Alzheimer’s disease; SVM, support vector machine; MMSE, Mini Mental State Examination; NINCDS-ADRDA, National Institute of Neurological and Communicative Disorders and Stroke/Alzheimer’s disease and related Disorders Association; LDDMM, Large Diffeomorphic Deformation Metric Mapping; MDS, Multi-Dimensional Scaling; GM, Gray matter; WM, White Matter; OASIS, Open Access Series of Imaging Studies; CDR, Clinical Dementia Rating

## 1. Introduction

Alzheimer’s disease (AD) is the most common form of dementia and usually diagnosed clinically from patient history and cognitive impairment testing [1]. Definitive diagnosis is hard to make until severe damage has occurred

in the cortex and neighboring areas. The cognitive impairment tests assess a patient’s cognitive and functional performance in eight areas: memory, language, perceptual skills, attention, constructive abilities, orientation, problem solving and functional abilities. The Mini-Mental State Examination (MMSE) is a widely used diagnosis tool to evaluate the cognitive impairment. The Clinical Dementia Rating (CDR) scale combining the MMSE along with the interviews with family members and caregivers is used to characterize and track a patient’s level of impairment [8, 12]. The diagnosis using such criteria is time-consuming, yet less than half of the AD patients are identified at an early time point in a primary care setting [14, 17]. Image-analysis methods therefore are required to help detect brain changes, or to help diagnose the illness before irreversible neuronal loss has set in [7].

To this end, several algorithms have been proposed. Kloppel et al. developed a supervised method using a support vector machine (SVM) in a high dimensional space, treating voxels as coordinates and the intensity value at each voxel as their location [10]. Trosset et al. proposed another semi-supervised learning method, which used multi-dimensional scaling (MDS) based on Large Diffeomorphic Deformation Metric Mapping (LDDMM) distance for embedding and linear discriminant analysis for training [15]. Ceyhan et al. analyze the shape and size of hippocampus, where prominent neuropathological markers are shown to be present in AD, and use hippocampal volume and LDDMM distance for detection [2].

In this paper, we propose an automatic unsupervised classification approach to distinguish AD from normal aging. The symmetric log-domain diffeomorphic demons algorithm [19] is used to compute the pair-wise registration of all brain MR images. The advantages of this algorithm are that the registration is symmetric with respect to the order of inputs and its output velocity field can be directly used in the Log-Euclidean domain. Then the deformation-based Riemannian distance is calculated between each pair of images to form an affinity matrix for the following spectral embedding method, which projects all the images onto a

low-dimensional space for further partitioning. In the final clustering, we use the quick shift method, which does not require assumptions about the data distribution or number of clusters.

Compared with existing methods, our approach is efficient and robust. The efficiency is due to the registration algorithm we select. We chose the symmetric log-domain diffeomorphic demons algorithm among the many existing methods since this algorithm is inverse consistent, and it gives the logarithms of diffeomorphisms for distance calculation directly. The robustness results from the pair-wise distance calculated from the pair-wise registration. Even though there are tissue differences (i.e. leukoaraiosis) between brains, pair-wise registration and distance use as much information as possible for a more informative embedding. Moreover, we can choose diffeomorphisms within various regions of interest (i.e. the whole brain, or the gray matter/white matter segmentation) when computing the distance, to find the best measurement distinguishing AD. Instead of performing grouping in the high-dimensional space as the SVM method [10], images here are clustered within a low-dimensional embedded space, where similarity relationships are represented spatially so that clusters are easier to visualize.

This paper is organized as follows. Background including the symmetric log-domain diffeomorphic demons registration, the spectral embedding, and the quick shift clustering are introduced from Section 2 to Section 4. Image based approaches are described in Section 5. In Section 6, we show our experimental results by applying the proposed method on a set of images from the OASIS database [11].

## 2. Symmetric log-domain diffeomorphic demons registration and distance calculation

Non-linear registration has been used in morphometric studies for characterizing and comparing anatomies or group analysis. The output deformation fields of non-linear registration algorithms are often required to be invertible and symmetric with respect to the order of the inputs [9, 16]. Another constraint on the deformation fields is that they should be diffeomorphic, meaning that the mapping should be continuous, smooth and bijective. Such deformation fields are called diffeomorphisms, and are elements of a Lie group. Vercauteren et al. proposed an algorithm called Symmetric Log-domain Diffeomorphic Demons that guarantees the above properties [19].

Define a smooth and continuous mapping  $\phi(\cdot)$  that best aligns a source image  $I_1(\cdot)$  with a target image  $I_0(\cdot)$ . The global energy function of diffeomorphic demons is:

$$E_{diffeo}(I_0, I_1, \phi, \mathbf{u}) = \|I_0 - (I_1 \circ \phi \circ \exp(\mathbf{u}))\| + \|\mathbf{u}\|^2. \quad (1)$$

where  $\mathbf{u}$  denotes the update field.

The algorithm starts with the initialization of  $\phi = Id$ , an identity transformation, and the optimization is performed within the space of diffeomorphisms using updates of the form  $\phi \circ \exp(\mathbf{u})$ . If  $\phi$  is represented as an exponential of a smooth velocity field  $\mathbf{v}$ , i.e.  $\phi = \exp(\mathbf{v})$ , then the diffeomorphic demons is extended to represent the complete spatial transformation in the log domain, becoming the log-domain diffeomorphic demons algorithm. The log-domain diffeomorphic demons algorithm defines the update rule as

$$\phi = \exp(\mathbf{v}) \leftarrow \exp(Z(\mathbf{v}, \mathbf{u})) \approx \exp(\mathbf{v}) \circ \exp(\mathbf{u}) = \phi \circ \exp(\mathbf{u}) \quad (2)$$

where  $Z(\mathbf{v}, \mathbf{u})$  is a velocity field. Since the update field  $\mathbf{u}$  is assumed to be small, the first order approximation of  $Z(\mathbf{v}, \mathbf{u})$  is computed by the Baker-Campbell-Hausdorff approximation:

$$Z(\mathbf{v}, \mathbf{u}) = \mathbf{v} + \mathbf{u} + \frac{1}{2} [\mathbf{v}, \mathbf{u}] + \frac{1}{12} [\mathbf{v}, [\mathbf{v}, \mathbf{u}]] + O(\|\mathbf{u}\|^2) \quad (3)$$

where  $[\mathbf{v}, \mathbf{u}]$  denotes a Lie bracket providing a velocity field defined at each voxel  $p$  by

$$[\mathbf{v}, \mathbf{u}](p) = \text{Jac}(\mathbf{v})(p) \cdot \mathbf{u}(p) - \text{Jac}(\mathbf{u})(p) \cdot \mathbf{v}(p). \quad (4)$$

After registration, the algorithm gives not only the deformation field  $\phi$ , but also the logarithm of the diffeomorphism,  $\mathbf{v} = \log(\phi)$ , which can be directly used in computational anatomical analysis.

The log-domain diffeomorphic demons registration has a symmetric (or inverse-consistent) extension [19]. The symmetry is obtained by symmetrizing the energy function:

$$\phi_{opt} = \underset{\phi}{\operatorname{argmin}} (E(I_0, I_1, \phi) + E(I_1, I_0, \phi^{-1})). \quad (5)$$

Starting from  $\phi = \exp(\mathbf{v})$  to minimize the first term  $E(I_0, I_1, \exp(\zeta))$ , one can get  $\zeta = K_{diff} * Z(\mathbf{v}, K_{fluid} * \mathbf{u}^{forw})$ , where  $\mathbf{u}^{forw}$  is the demons force,  $K_{diff}$  and  $K_{fluid}$  are diffusion-like and fluid-like Gaussian convolution kernels, respectively. Similarly, the second term  $E(I_1, I_0, \exp(-\tau))$  is optimized with  $\tau = K_{diff} * Z(\mathbf{v}, K_{fluid} * \mathbf{u}^{back})$ , where  $\mathbf{u}^{back}$  is the demons force for reversed inputs.

In general, the symmetric log-domain diffeomorphic demons registration algorithm [19] is:

*Algorithm 1 (Symmetric log-domain diffeo demons)*

- Choose a starting spatial transformation  $\phi = \exp(\mathbf{v})$
- Iterate until convergence:
  - Compute the demons force  $\mathbf{u}^{forw}$  to minimize  $E(I_0, I_1, \exp(\mathbf{v}), \mathbf{u}^{forw})$

- Compute the demons force  $\mathbf{u}^{back}$  to minimize  $E(I_1, I_0, \exp(-\mathbf{v}), \mathbf{u}^{back})$
- For fluid-like regularization, let  $\mathbf{u} \leftarrow \frac{1}{2} K_{fluid} * (\mathbf{u}^{forw} - \mathbf{u}^{back})$
- For diffusion-like regularization, let  $\mathbf{v} \leftarrow K_{diff} * (\mathbf{v} + \mathbf{u})$  else let  $\mathbf{v} \leftarrow \mathbf{v} + \mathbf{u}$  ■

The algorithm outputs the final deformation field  $\phi$ , which is a diffeomorphism, after convergence. Readers can refer to the work of Vercauteren et al. [19] for more details on the symmetric log-domain diffeomorphic demons registration.

To compute the distance between images, Riemannian distance is defined [5]. The Riemannian distance between two points from a Lie group  $\mathcal{G}$  is defined by

$$dist(a, b) = \|\log(a^{-1}b)\|, \quad a, b \in \mathcal{G} \quad (6)$$

For each pair of images  $\{I_j, I_k\}$ , the symmetric log-domain diffeomorphic demons algorithm gives a mapping  $\phi$  from  $I_k$  to  $I_j$ , a velocity field  $\mathbf{v} = \log(\phi)$  (that is,  $\phi = \exp(\mathbf{v})$ ), and an inverse mapping  $\phi^{-1} = \exp(-\mathbf{v})$  from  $I_j$  back to  $I_k$ . The following Eq.(7) is used to compute the Riemannian distance between  $I_j$  and  $I_k$ :

$$\begin{aligned} dist(I_j, I_k) &= dist(Id, \phi) = dist(\phi^{-1}, Id) \\ &= \|\log(Id^{-1}\phi)\| \\ &= \|\log(\phi)\| \\ &= \|\log[(\phi^{-1})^{-1}Id]\| \\ &= \|\mathbf{v}\| \end{aligned} \quad (7)$$

where  $Id$  denotes an identity transformation.

In Eq.(7),  $\phi$  is a diffeomorphism mapping between the whole images  $I_j$  and  $I_k$ . In this paper, we define the regional distance between  $I_j$  and  $I_k$  as follows:

$$\begin{aligned} REGdist(I_j, I_k) &= REGdist(Id, \phi) \\ &= (\|\log(\phi)\|)_{\Omega} \\ &= \int_{\Omega} \|v(p)\| dp \end{aligned} \quad (8)$$

where  $\phi$  denotes the diffeomorphism mapping from  $I_k$  to  $I_j$ ,  $\Omega$  denotes the regions of interest, such as the whole brain, gray matter, white matter, cortical lobes or subcortical structures,  $p$  denotes the voxels in  $\Omega$ , and  $v = \log(\phi)$ . If  $\Omega$  represents the whole brain, the distance calculated is called the whole-brain distance. If  $\Omega$  represents the gray matter region, the distance calculated is called the gray matter (GM) distance, with similar notation for other regions of interest.

### 3. Spectral embedding

Spectral methods [6, 13] for clustering are based on the ranked eigenvectors of an  $N \times N$  matrix derived from the

affinity or distance between subjects.  $N$  denotes the number of subjects in the test dataset. The eigenvectors induce an embedding of the subjects in a low-dimensional subspace wherein a simple central clustering method can then be used to do the final partitioning.

Given a set of subjects  $S = \{s_1, s_2, \dots, s_N\}$  in  $\mathbb{R}^d$ , distance matrix is first computed with diagonal entries to be zeros. Distances are then converted to affinities through a Gaussian kernel:

$$a_{jk} = \exp(-dist^2(I_j, I_k)/2\sigma^2) \quad (9)$$

The affinity matrix  $A \in \mathbb{R}^{N \times N}$ , where  $N$  is the number of images in the dataset, is defined by:

$$A = \begin{cases} \exp(-dist^2(I_j, I_k)/2\sigma^2) & \text{if } j \neq k \\ 0 & \text{if } j = k \end{cases} \quad (10)$$

With the affinity matrix calculated above, all images in the dataset can be projected onto a low-dimensional space after the following steps. Eigenvalue decomposition is performed on the normalized Laplacian matrix  $\mathcal{L}$ , which is defined as

$$\mathcal{L} = D^{-1/2}(A - D)D^{-1/2} = D^{-1/2}AD^{-1/2} \quad (11)$$

where  $D$  is the diagonal matrix with entries  $D_{ij} = \sum_j A_{ij}$ . We then select  $k$  leading eigenvectors and compute the  $N \times k$  matrix  $V$  to embed each image onto a  $k$ -dimensional Euclidean space, with  $k \ll N$ . The  $j$ th embedding coordinate of the  $i$ th image is then given by

$$E_{ij} = \frac{V_{ij}}{\sqrt{\sum_j V_{ij}^2}} \quad (12)$$

where the eigenvectors have been sorted in descending order by eigenvalues. Thus, each image is associated with a row of  $E$  and they are treated as samples  $\{x_1, \dots, x_N\}$  in the following clustering method.

### 4. Quick shift clustering

In the mode seeking problem, mean shift [3] is known as a popular non-parametric clustering algorithm based on the idea of associating each data point to a mode of the underlying probability density function. Quick shift [18] is an extension on the mean shift method exploiting kernels to a non-Euclidean setting.

Given  $N$  data points  $x_1, \dots, x_N \in \mathcal{X} = \mathbb{R}^d$ , a mode seeking clustering algorithm [18] conceptually starts by computing the Parzen density estimate

$$P(x) = \frac{1}{N} \sum_{i=1}^N \psi(x - x_i), \quad x \in \mathbb{R}^d \quad (13)$$

where  $\psi(x)$  can be a Gaussian kernel (i.e.  $\psi(x) = c \cdot \exp(-\|x\|^2/2\sigma^2)$ ) or other kernels. Each point  $x_i$  is moved towards a mode of  $P(x)$  evolving the trajectory  $y_i(t)$ ,  $t > 0$ .

The main idea of quick shift is to move each point  $x_i$  to the nearest neighbor with higher density  $P(x)$ . The current position of  $x_i$  is denoted by  $y_i(0)$ . The next position of  $x_i$ ,  $y_i(1)$ , is computed by:

$$y_i(1) = \operatorname{argmin}_{j:P_j > P_i} D_{ij}, \quad P_i = \frac{1}{N} \sum_{j=1}^N \dot{\psi}(D_{ij}) \quad (14)$$

where  $D_{ij} = d(x_i, x_j)$  and  $\dot{\psi}$  is the derivative of  $\psi$ . To balance under- and over-fragmentation of the modes, quick shift can be slightly modified by introducing a threshold parameter  $\tau$  into Eq.(14):

$$y_i(1) = \operatorname{argmin}_{\substack{j : P_j > P_i \\ D_{ij} < \tau}} D_{ij}, \quad P_i = \frac{1}{N} \sum_{j=1}^N \dot{\psi}(D_{ij}) \quad (15)$$

For each point, the next position as well as the evolution trajectory is computed. All points converging to the same mode finally form a cluster.

Quick shift has many advantages:

- The simplicity and speed;
- The structure of the clusters may be rather arbitrary;
- The number of clusters does not need to be known in advance;
- The data space  $\mathcal{X}$  can be non-Euclidean;

## 5. Image based clustering

Given a set of images  $I_1, I_2, \dots, I_N$ , pair-wise registration is performed using the symmetric log-domain diffeomorphic demons algorithm with default parameters [19]. Each diffeomorphism output from registration is used to compute the whole-brain distance or other regional distance. The distance matrix is constructed after pair-wise distance is calculated, with zero diagonal entries. The spectral embedding is then applied to project all the images onto an  $\mathbb{R}^k$  space, where the quick shift clustering method is employed to group the images. In the spectral embedding,  $k$  is manually selected from  $2 \sim 15$ . In this paper, results with  $k = 3$  are shown in Section 6 since the clustering results using other  $k$  values are no better than that using  $k = 3$ , and the clustering procedure can be better illustrated when  $k = 3$ .

In general, the image-based clustering algorithm is

*Algorithm2 (Image-based clustering algorithm)*

Given a set of images  $\{I_1, I_2, \dots, I_N\}$ ,

- Compute the pair-wise registration using the symmetric log-domain diffeomorphic demons algorithm;
- Compute the pair-wise distance and construct the distance matrix;
- All images are projected onto an  $\mathbb{R}^k$  subspace using the spectral embedding method with manually selected  $k$ ;
- Quick shift unsupervised clustering method is performed in the constructed subspace. Images are partitioned into sub-groups.

## 6. Experiments and results

We used MR images from the Open Access Series of Imaging Studies (OASIS) database [11]. The OASIS data set consists of a cross-sectional collection of 416 subjects aged 18 to 96 years. One hundred of the included subjects older than 60 years have been clinically diagnosed with very mild to moderate Alzheimer’s disease. The subjects are all right-handed and include both men and women. For each subject, 3-4 individual T1-weighted magnetization prepared rapid gradient-echo (MR-RAGE) images were acquired on a 1.5-T Vision scanner in a single imaging session. In our experiments, 75 subjects are selected from the OASIS database, including 35 subjects (age 69~96) with very mild to mild dementia and 40 age-matched control subjects (age 67~91) with no sign of clinical dementia at the time of scanning (Table 1). The diseased subjects are clinically diagnosed and characterized using the Clinical Dementia Rating (CDR) scale [12], which considers both the Mini-Mental State Examination (MMSE) and the necessary information from patients’ family members or caregivers. This score is used to characterize and to track a patient’s level of impairment:

- 0 = Normal
- 0.5 = Very Mild Dementia
- 1 = Mild Dementia
- 2 = Moderate Dementia
- 3 = Severe Dementia

	Normal Group	Diseased Group
mean age(range)	77.275(67~91)	80.371(69~96)
MMSE	26~30	15~29
CDR scale	0	0.5~1

Table 1. Age and diagnosis characteristics of the test dataset

The classification based on the CDR scale is used as the groundtruth in our experiments. All the images have already been affinely transformed to a standard coordinate frame, bias corrected, and skull stripped for analysis. The segmentations of the whole brain, gray matter and white matter

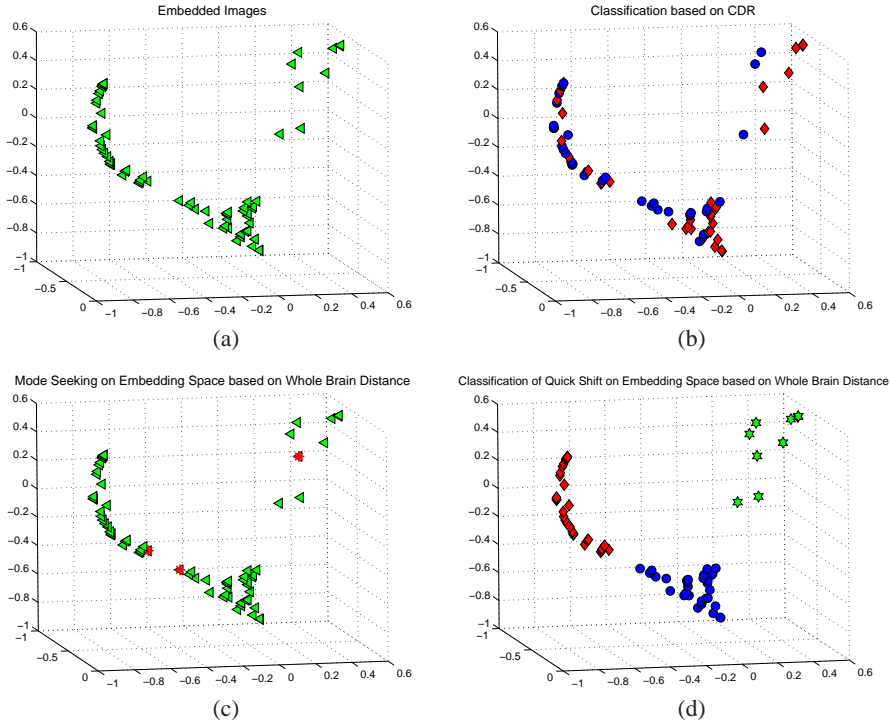


Figure 1. Classification on dataset using the whole-brain distances. (a) 75 brains are projected onto  $\mathbb{R}^3$  space via spectral embedding; (b) Classification according to the CDR scale, with red diamonds representing the brains of cognitively normal controls and blue circles representing the brains of patients with AD; (c) Three modes denoted by red stars are found by the quick shift method in the embedded space; (d) Quick shift classification result in the embedded space.

are provided by the OASIS database. Other segmentations, such as hippocampus, are obtained using the FreeSurfer [4] software.

The parameter  $\sigma$  in Eq. 9 is set in the same range as the corresponding distance. The strategy used here is to set  $\sigma$  to be the mean of the distances, then manually adjust the value up and down to obtain a best projection. The kernel  $\psi$  in Eq. 13 is used to compute the Parzen density for the quick shift clustering. The  $\sigma$  and  $c$  are both set to be 1. The  $\tau$  in Eq. 15 is set 0.5.

In the first test, we use the distances computed from the whole brain diffeomorphisms for spectral embedding. For  $k = 3$ , all images are projected onto an  $\mathbb{R}^3$  Euclidean space (Fig 1(a)). Then quick shift clustering is performed to discover the subgroups (Fig 1(c)(d)).

With the whole-brain distance, the embedded images are not quite separable (Fig 1(b)). The classification result using the spectral embedding plus quick shift method (Fig 1(d)) is not in accordance with the classification based on the CDR scale (Fig 1(b)).

In the second test, we use the gray matter distance, which is computed from diffeomorphisms of gray matter segmentations using Eq. 8, instead of the whole-brain distance for embedding (Fig 2(a)). Then quick shift method is applied in the embedded space (Fig 2(c)(d)).

With the gray matter distance, the embedded images are much more separable (Fig 2(b)). The classification result of our method is almost identical with the classification based on the CDR scale, except that one 71 year old AD patient with an MMSE of 27 and one 83 year old patient are misclassified into the control group.

The white matter distance is used for embedding and clustering in the third test (Fig 3). Two normal subjects and two AD patients are misclassified.

We used the whole-brain distance in our earlier experiments, not presented here, to partition young brains and elderly brains that are also obtained from the OASIS database, using exactly the same approaches proposed in this paper. While it works very well for grouping the young and elderly brains, it fails to differentiate AD from normal aging in the experiment presented here, indicating that overall brain changes occur obviously as aging but there are no large global changes between normal aging persons and AD patients. The deformation found in the gray matter via registration is observed to be able to better characterize the brain changes of AD patients in our experiment, or in other words, it is a better metric to distinguish AD from normal aging. This result is consistent with the strong evidence that AD is characterized by gray matter atrophy. Since white matter and gray matter are adjacent, any changes or defor-

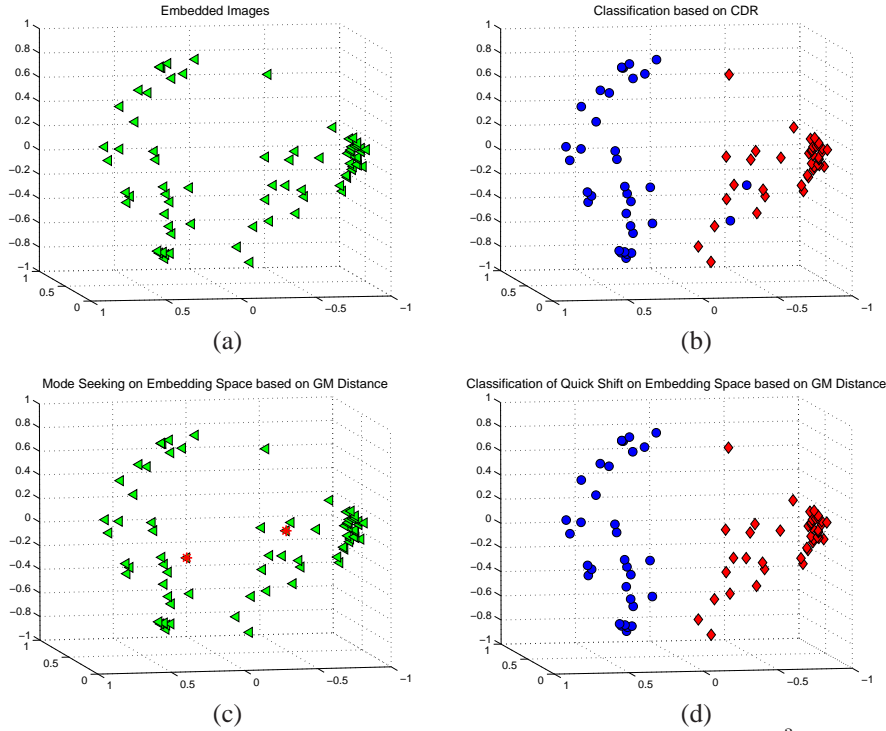


Figure 2. Classification on dataset using the gray matter distances. (a) 75 brains are projected onto  $\mathbb{R}^3$  space via spectral embedding; (b) Classification according to the CDR scale, with red diamonds representing the brains of cognitively normal controls and blue circles representing the brains of patients with AD; (c) Two modes denoted by red stars are found by the quick shift method in the embedded space; (d) Quick shift classification result in the embedded space.

Method	Target structure	Correctly classified(%)
MDS	hippocampus	60~75
SVM	gray matter	85.6~95.6
Our method	gray/white matter	94.67~97.33

Table 2. Result comparisons.

mations occurring in gray matter could result in changes or deformations in nearby white matter. Therefore, the white matter distance works better than the whole-brain distance, but slightly worse than the gray matter distance in distinguishing subjects.

In the fourth test, the hippocampus distance is used for embedding. Although hippocampal volume has shown to be a sensitive marker for AD in some studies of temporal lobe structures, the hippocampus distance used in our experiment does not provide the most separable projection for grouping, giving a correct classification rate of 88% (Fig 4).

Using the white matter distance, 94.67% of subjects are correctly assigned to the appropriate group. A further improvement to 97.33% was obtained when the gray matter distance is used, which is better than the results shown in MDS method [15] and comparable to the results illustrated in SVM method [10] (Table2).

In addition, the brain MR images used in our experiments are taken from patients with very mild to mild dementia. Thus we believe that the algorithm we proposed in this paper can help early diagnosis in Alzheimer’s disease.

The source code of the symmetric log-domain diffeomorphic demons registration can be downloaded from <http://www.insight-journal.org/browse/publication/644>. Other source code for reproducing the results are also available online - see <http://www.bsl.ece.vt.edu/ReproducibleResearch/CVPR10-Clustering>.

## 7. Conclusion

In this paper, we propose a method to effectively differentiate AD from normal aging. In our method, the symmetric log-domain diffeomorphic demons registration is used to compute the pair-wise registration. Since this algorithm is inverse consistent with respect to the order of input images, for each pair the registration need only be computed once. With another advantage that the outputs of the log-domain diffeomorphic demons registration include not only the deformation field but also its log field, so that the heavy computation of the log of the spatial transformation is no longer required. The Riemannian distances that quantify

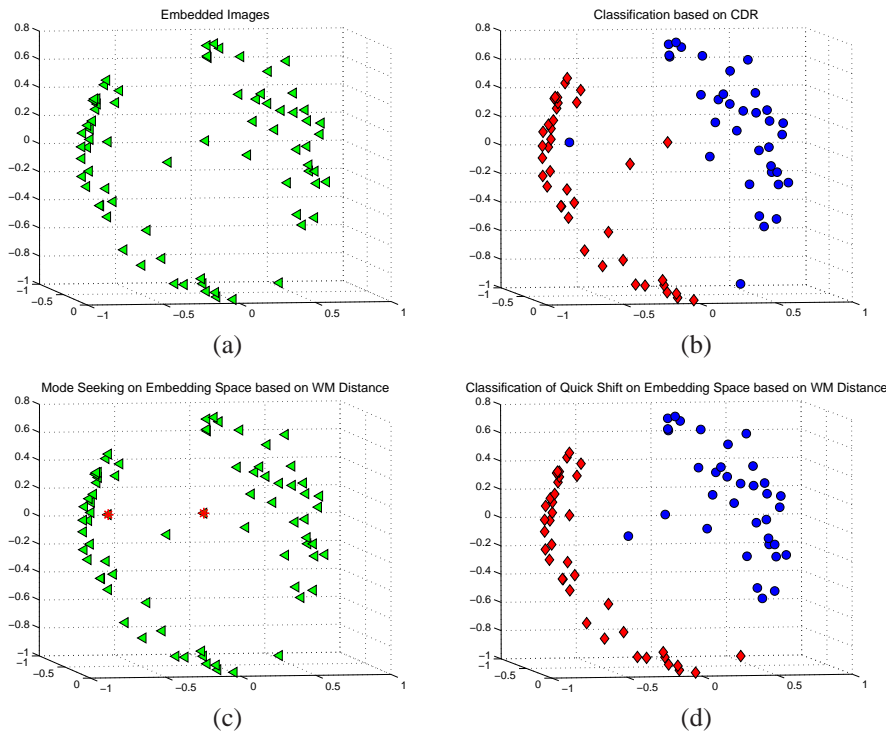


Figure 3. Classification on normal and diseased dataset using the white matter distances. (a) 75 brains are projected onto  $\mathbb{R}^3$  space via spectral embedding; (b) Classification according to the CDR scale, with red diamonds representing the brains of cognitively normal controls and blue circles representing the brains of AD patients; (c) Two modes denoted by red stars are found by the quick shift method in the embedded space; (d) Quick shift classification result in the embedded space.

the pair-wise diffeomorphisms form the distance matrix, which is latter converted to be an affinity matrix through a Gaussian kernel. The spectral embedding of all images in the dataset is performed based on the image affinity values. In the embedded space each image is represented as a point, and nearby points in general correspond to images of high anatomical similarity. The advantage of this space is that similarity relationships are represented spatially, so that clusters can be more easily found. Quick shift, an efficient clustering method with no data distribution assumptions, is finally employed for partitioning in the embedded space in this work.

We apply the proposed method to a subset of images selected from the OASIS database using the whole-brain distance, the gray matter distance, the white matter distance and the hippocampus distance, respectively. It is observed that the gray matter distance can best separate the AD patients from the cognitively normal controls. And we believe that this algorithm could help early diagnosis of the disease.

## Acknowledgement

This research was funded by the National Institutes of Health through the National Institute on Drug Abuse, Grant R01-DA020648-01; and the NIH Roadmap for Medical Re-

search, Grant U54 RR021813.

## References

- [1] K. Blennow, M. de Leon, and H. Zetterberg. Alzheimer's disease. *Lancet*, 368:387–403, 2006.
- [2] E. Ceyhan, C. Ceritoglu, and et al. Analysis of metric distances and volumes of hippocampi indicates different morphometric changes over time in dementia of alzheimer type and nondemented subjects. *Technical Report*, Department of Mathematics, Koc University, Istanbul, Turkey, 2008.
- [3] Y. Cheng. Mean shift, mode seeking, and clustering. *IEEE Trans. Pattern Analysis and Machine Intelligence*, 17:790–799, 2008.
- [4] A. Dale, B. Fischl, and M. Sereno. Cortical surface-based analysis i: Segmentation and surface reconstruction. *NeuroImage*, 9(2):179–194, 1999.
- [5] P. T. Fletcher, C. Lu, and S. Joshi. Statistics of shape via principal component analysis on lie group. *In Proceedings of CVPR*, 2003.
- [6] C. Fowlkes, S. Belongie, F. Chung, and J. Malik. Spectral grouping using the nystrom method. *IEEE Transactions on Pattern Analysis and Machine Intelligence*, 26:214–225, 2004.
- [7] N. Fox and J. Schott. Imaging cerebral atrophy: normal ageing to alzheimer's disease. *Lancet*, 363:392–394, 2004.

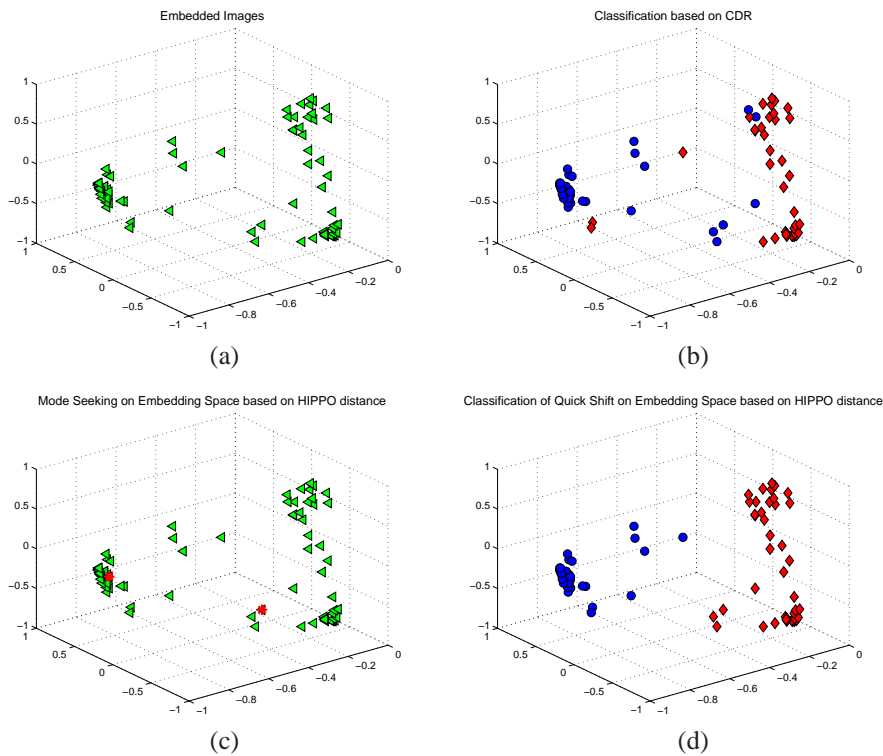


Figure 4. Classification on normal and diseased dataset using the hippocampus distances. (a) 75 brains are projected onto  $\mathbb{R}^3$  space via spectral embedding; (b) Classification according to the CDR scale, with red diamonds representing the brains of cognitively normal controls and blue circles representing the brains of AD patients; (c) Two modes denoted by red stars are found by the quick shift method in the embedded space; (d) Quick shift classification result in the embedded space.

- [8] P. Harvey, P. Moriarty, L. Kleinman, and et al. The validation of a caregiver assessment of dementia: the dementia severity scale. *Alzheimer Dis Assoc Disord*, 19:186–194, 2005.
- [9] S. Joshi, B. Davis, M. Jomier, and G. Gerig. Unbiased diffeomorphic atlas construction for computational anatomy. *Neuroimage*, 23:151–160, 2004.
- [10] S. Kloppel, C. Stonnington, and et al. Automatic classification of mr scans in alzheimer’s disease. *Brain*, 131:681–689, 2008.
- [11] D. Marcus, T. Wang, J. Parker, J. Csernansky, J. Morris, and R. Buckner. Open access series of imaging studies (oasis); cross-sectional mri data in young, middle aged, non-demented, and demented older adults. *J Cog Neurosci*, 19:1498–1507, 2007.
- [12] J. Morris. The clinical dementia rating(cdr): Current version and scoring rules. *Neurology*, 43:2412–2414, 1993.
- [13] A. Ng, M. Jordan, and Y. Weiss. On spectral clustering: Analysis and an algorithm. *Advances in Neural Information Processing Systems*, 14, 2001.
- [14] P. Solomon and C. Murphy. Should we screen for alzheimer’s disease? a review of the evidence for and against screening alzheimer’s disease in primary care practice. *Geriatrics*, 60:26–31, 2005.
- [15] M. Trosset, C. Priebe, Y. Park, and M. Miller. Semisupervised learning from dissimilarity data. *Technical Report*, Department of Statistics, Indiana University, Bloomington, IN4705, 2007.
- [16] M. Vaillant, M. Miller, L. Younes, and A. Trounev. Statistics on diffeomorphisms via tangent space representations. *Neuroimage*, 23:161–169, 2004.
- [17] V. Valcour, K. Masaki, J. Curb, and P. Blanchette. The detection of dementia in the primary care setting. *Arch Intern Med*, 160:2964–2968, 2000.
- [18] A. Vedaldi and S. Soatto. Quick shift and kernel methods for mode seeking. *ECCV, Part IV. LNCS*, 5305:705–718, 2008.
- [19] T. Vercauteren, X. Pennec, A. Perchant, and N. Ayache. Symmetric log-domain diffeomorphic registration: A demons-based approach. *MICCAI, LNCS*, 5241:754–761, 2008.